

A history of mild shocks experienced by the regolith particles on hydrated asteroid Ryugu

Received: 12 May 2022

Accepted: 16 March 2023

Published online: 20 April 2023

 Check for updates

Naotaka Tomioka¹✉, Akira Yamaguchi^{2,3}, Motoo Ito¹, Masayuki Uesugi⁴, Naoya Imae^{2,3}, Naoki Shirai^{5,6}, Takuji Ohigashi^{7,8}, Makoto Kimura², Ming-Chang Liu^{9,21}, Richard C. Greenwood¹⁰, Kentaro Uesugi⁴, Aiko Nakato¹¹, Kasumi Yogata¹¹, Hayato Yuzawa⁷, Yu Kodama^{12,22}, Kaori Hirahara¹³, Ikuya Sakurai¹⁴, Ikuo Okada¹⁴, Yuzuru Karouji¹¹, Keishi Okazaki^{1,15}, Kosuke Kurosawa¹⁶, Takaaki Noguchi¹⁷, Akira Miyake¹⁷, Masaaki Miyahara¹⁵, Yusuke Seto¹⁸, Toru Matsumoto¹⁷, Yohei Igami¹⁷, Satoru Nakazawa¹¹, Tatsuaki Okada¹¹, Takanao Saiki¹¹, Satoshi Tanaka¹¹, Fuyuto Terui¹⁹, Makoto Yoshikawa¹¹, Akiko Miyazaki¹¹, Masahiro Nishimura¹¹, Toru Yada¹¹, Masanao Abe¹¹, Tomohiro Usui¹¹, Sei-ichiro Watanabe²⁰ & Yuichi Tsuda^{3,11}

Micrometeorites, a possible major source of Earth's water, are thought to form from explosive dispersal of hydrated chondritic materials during impact events on their parental asteroids. However, this provenance and formation mechanism have yet to be directly confirmed using asteroid returned samples. Here, we report evidence of mild shock metamorphism in the surface particles of asteroid Ryugu based on electron microscopy. All particles are dominated by phyllosilicates but lack dehydration textures, which are indicative of shock-heating temperatures below ~500 °C. Microfault-like textures associated with extensively shock-deformed framboidal magnetites and a high-pressure polymorph of Fe–Cr–sulfide have been identified. These findings indicate that the average peak pressure was ~2 GPa. The vast majority of ejecta formed during impact on Ryugu-like asteroids would be hydrated materials, larger than a millimetre, originating far from the impact point. These characteristics are inconsistent with current micrometeorite production models, and consequently, a new formation mechanism is required.

Hypervelocity collisions between small bodies were a frequent occurrence in the early Solar System¹, resulting in a variety of outcomes such as brecciation, cratering, accretion, magma generation and degassing². These processes have been recorded as a wide variety of physical and chemical modifications to asteroidal and planetary surface materials, including brittle/plastic deformation structures, solid-state phase

transformations, recrystallization, melting and vaporization². Therefore, planetary material scientists have been enthusiastically investigating shocked meteorites, which are thought to be derived from asteroids, the Moon and Mars³, to understand the nature of the impact events and related processes that have taken place throughout the Solar System's history^{4–6}. For instance, peak pressure and its duration decoded from

A full list of affiliations appears at the end of the paper. ✉ e-mail: tomioka@jamstec.go.jp

shocked meteorites provide constraints on past collisional velocities and also, the sizes of asteroids^{7,8}.

To link such impact event parameters to well-defined Solar System environments, knowledge of the relevant source regions is required. However, at present, there are only limited numbers of returned samples available for detailed study. Shock effects have been reported in lunar rocks returned by the Apollo missions^{9,10}, cometary nucleus materials returned by the Stardust mission^{11,12}, and the surface particles of the S-type asteroid Itokawa returned by the Japan Aerospace Exploration Agency (JAXA) Hayabusa mission. In Itokawa particles, shock-induced defect structures (crystal lattice dislocations), melt splash, and microcraters were first identified in olivine grains^{13,14}. The shock effects of the entire Itokawa rock could not be fully evaluated, despite some attempts based on crystallographic and spectroscopic analyses of olivine and plagioclase^{15,16}. This is because most of the returned particles consist of single grains or aggregates of several grains only <50 μm in size.

Shock effects related to hydrated asteroids are of particular interest in planetary sciences as such asteroids are thought to be one of the major sources of extraterrestrial dust particles¹⁷. The bulk of extraterrestrial material arriving on Earth comes in the form of micrometeorites in the size range of 50–500 μm¹⁸, with an estimated flux of ~30,000 tons per year¹⁹. Most unmelted and partially melted micrometeorites are similar in chemistry and mineralogy to the matrices of CI (Ivuna-type), CM (Mighei-type) and Tagish Lake-type carbonaceous chondrites, which are porous aggregates composed mainly of hydrous phyllosilicates^{20,21}. Such materials are likely to be explosively pulverized to become micrometeorites by the vaporization of volatile components, like H₂O, during shock heating and therefore, are unlikely to survive as meteorites²². This hypothesis was further confirmed by comparing the petrology and mineralogy of recovered samples of anhydrous CV (Vigarano-type) and hydrated CM chondritic meteorites using laboratory shock experiments^{23,24}.

JAXA's Hayabusa2 mission has provided an opportunity to directly evaluate the shock metamorphism of hydrated asteroidal materials. The Hayabusa2 spacecraft successfully brought back to Earth approximately 5.4 g of total material from the C-type asteroid 162173 Ryugu in early December 2020²⁵. The returned materials include Ryugu's surface particles collected by the first touchdown (chamber A particles) and the second touchdown near the artificial impact crater (chamber C particles) formed by the small carry-on impactor (SCI)²⁵. The present study aims to evaluate the degree of shock metamorphism of Ryugu's surface materials by scanning electron microscopy (SEM) and transmission electron microscopy (TEM) and to assess the hypothesis that massive dust production is driven by dehydration during impact processing on small hydrated Solar System bodies, including Ryugu.

Results

In the present study, we investigated five Ryugu particles (A0002, A0037, C0009, C0014 and C0068) from both chambers A and C using SEM and/or TEM. The mineralogy and petrology as well as the elemental and isotopic compositions of the Ryugu particles^{26–33} have close similarities with the CI chondritic meteorites^{34–36}. The present study mainly focuses on the shock features of Ryugu particles observed using electron microscopy.

The Ryugu particles examined in this study initially appeared unshocked; however, we found some characteristic features related to shock metamorphism. The observed bulk particles have irregular fractures, especially in those examples that are particularly carbonate rich^{27,32}. Subparallel fractures, which have been reported in experimentally shocked hydrated CM chondrites³⁷, were not observed (Fig. 1a). Another possible shock-related feature observed in SEM is the brittle deformation of olivine grains. In particle C0009, more than 10 grains of isolated olivine were identified in the phyllosilicate matrix^{28,32}. The olivine grains (<50 μm) partly exhibit irregular fractures but do

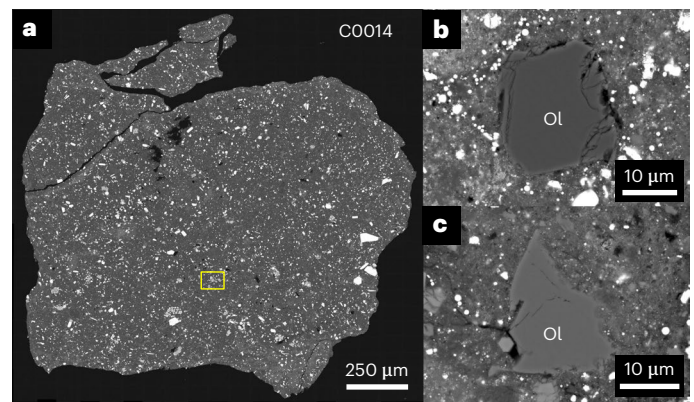


Fig. 1 | Representative petrography of Ryugu particles. **a**, Backscattered electron (BSE) image of the polished section of particle C0014. Fe sulfide and oxide grains (bright portions) are embedded in the phyllosilicate-rich matrix (dark grey). The particles only have some irregular fractures. The boxed area is shown in Fig. 2a. **b, c**, BSE images of two different olivine grains (Ols) in particle C0009. Both of the Ols show some irregular fractures but do not show planar fractures, which are formed by peak pressures only above ~5 GPa.

not show planar fractures, as found in experimentally and naturally shocked olivines² (Fig. 1b,c).

Shock-induced melt veins and melt pockets are absent in all particles. However, particle C0014 exhibits rare, thin, straight veins less than 70 μm in length and less than 5 μm in width. In one of these veins, an aggregate of spherical magnetite particles has a thin lens shape, and the aggregate is terminated on both sides by elongated phyllosilicates along the veins (Fig. 2a,b). The phyllosilicate vein contains neither vesicles nor Fe–Ni–S nanoglobules, which are known to represent dehydration/melting products³⁷. The chemical composition of the phyllosilicates is nearly the same as that of the fine-grained phyllosilicate matrix (Fig. 2c). Along the same direction as the vein, another framboidal magnetite aggregate is deformed in simple shear (Fig. 2a,b).

Four Ryugu particles (A0002, A0037, C0009 and C0068) were further examined at a higher spatial resolution by TEM. The ultrathin sections extracted from the above particles consist mainly of phyllosilicates containing Fe sulfides and Fe oxide grains (Fig. 3a and Supplementary Figs. 1 and 2). Coarse-grained phyllosilicate aggregates of several micrometres in size occur with feathery textures embedded in fine-grained phyllosilicate matrices. The high-resolution TEM image and selected-area electron diffraction (SAED) patterns clarified that the phyllosilicates are intergrown serpentine and saponite, with interlayer spacings of 0.7 and 1.1 nm, respectively (Fig. 3b). Portions of the fine matrix phyllosilicates are poorly crystalline, showing diffraction rings with *d* spacings of 0.45, 0.25 and 0.15 nm (Fig. 3c). The chemical compositions of coarse- and fine-grained phyllosilicates in particles A0037 and C0068 have an Mg/(Mg + Fe) atomic ratio of 0.84 ± 0.03 (1σ) (Fig. 3d and Supplementary Table 1), while those of phyllosilicates in A0002 and C0009 are more toward the Fe end member. Fe enrichment could be caused by extremely fine (<10 nm) Fe sulfide particles embedded in the phyllosilicates and/or Mg–Fe heterogeneity within the phyllosilicates. These values are consistent with those of phyllosilicates in other Ryugu particles^{31,33} and the Orgueuil CI chondrite³⁴.

Pyrrhotite and magnetite are the second most abundant minerals after the phyllosilicates. Pyrrhotite generally occurs as euhedral and subhedral grains up to 6 μm in size throughout the fine-grained phyllosilicate matrix (Supplementary Figs. 2 and 3a,c,e). Magnetite occurs mostly as isolated spherical grains (<8 μm) or aggregates of spherical grains (<0.9 μm) corresponding to 'framboids' in CI chondrites (Supplementary Figs. 2c and 3c). Pentlandite occurs as smaller grains (<0.8 μm

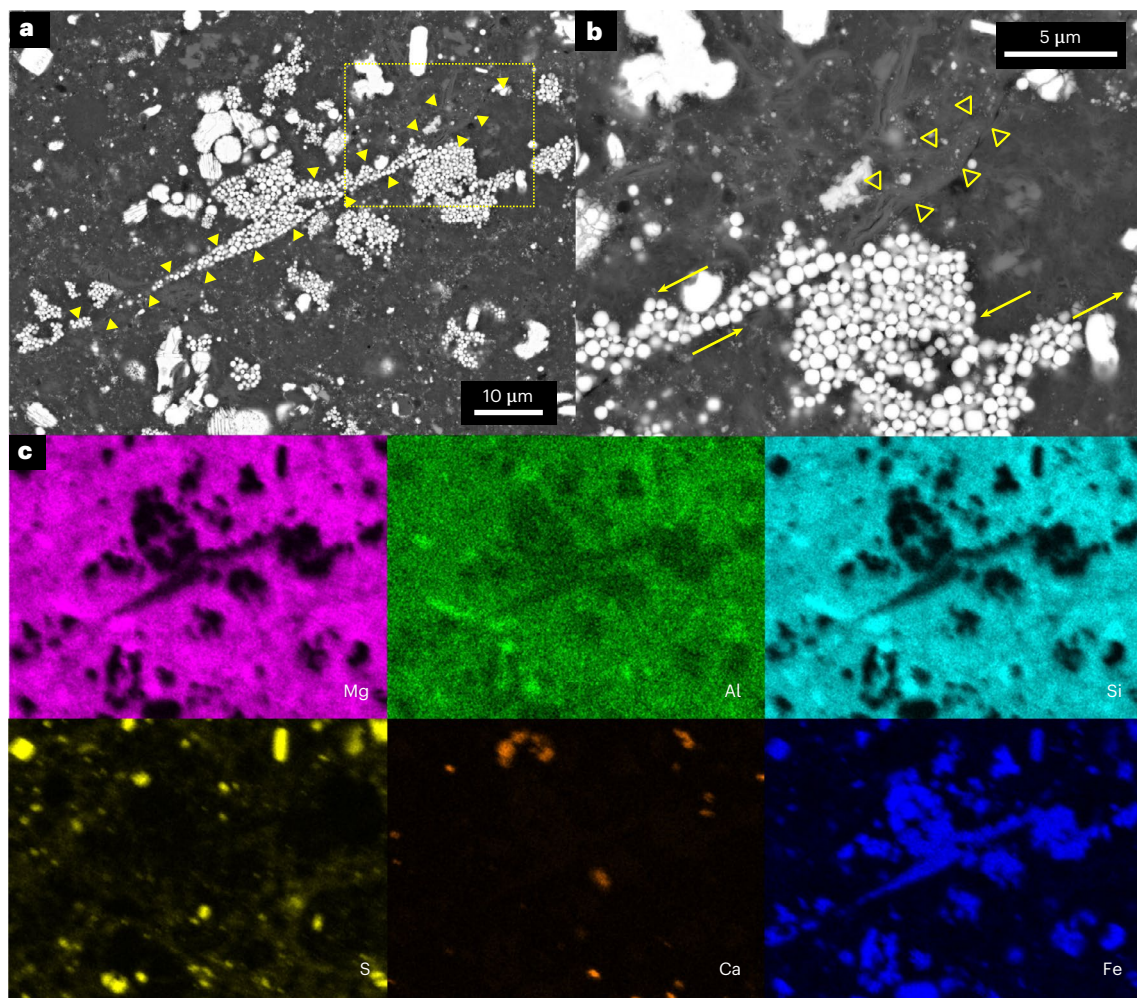


Fig. 2 | Microfault-like microstructures in particle C0014. **a**, BSE image of a microshear zone (indicated by filled yellow triangles). A framboidal magnetite aggregate is elongated along the shear zone. **b**, Magnified image of the boxed area in **a**. Arrows indicate the shear directions along the microfault in **a** and another fault offset of a framboidal magnetite aggregate. An elongated

phyllosilicate grain along the microfault is indicated by open yellow triangles. **c**, X-ray maps of Mg, Al, Si, S, Ca and Fe of the area in **a**. The silicate portion along the microfault has similar chemical composition to that of the surrounding silicate matrix. The absences of vesicles and Fe–Ni–S globules in the fault zone suggest that the portion was not melted by shock heating.

in size) than magnetite and pyrrhotite (Supplementary Figs. 2 and 3e). Minor eskolaite (Cr_2O_3 ; $<0.8 \mu\text{m}$ in size) were also found in particles C0009 and C0068 (Supplementary Figs. 2c and 3g).

Notably, a unique Fe sulfide grain was observed in A0002 (Fig. 4a). This grain is euhedral and $1.2 \mu\text{m}$ in size with a pure FeCr_2S_4 composition (Fig. 4b), and it is located within the fine-grained phyllosilicate matrix (Supplementary Fig. 2a). This type of sulfide is known as daubréelite and has a cubic spinel structure. However, SAED patterns from the grain are indexed only with a monoclinic FeCr_2S_4 phase known as a mineral zolenskyite, which was recently discovered in an enstatite chondrite³⁸ (Fig. 4c,d and Methods).

Discussion

Progressive petrographic and mineralogical transitions are used to classify meteorites and terrestrial impact crater rocks². Brittle deformation features in bulk particles and their constituent minerals are criteria related to relatively low-shock grades in chondritic meteorites (shock stages S1–S3)^{2,37}. This classification proposes that subparallel fractures in bulk meteorites and planar fractures in olivine grains are indicators of peak pressures above 15 (ref. 37) and 5 GPa (ref. 2), respectively. Hence, the absence of these types of fractures suggests that the peak pressure for Ryugu particles was lower than 5 GPa.

In the present study, we report a new constraint on peak pressure using a microfault-like vein found in particle C0014. The vein lacks any melting microtextures that are commonly observed in strongly shocked meteorites, such as vesicles and Fe–Ni–S nanoglobules^{6,37}. The latter is evidence of a quenched mixture of immiscible silicate and metal sulfide melts. Therefore, this feature in C0014 is likely a fine-grained lithic vein formed by brittle cataclastic deformation. The elongation and offset of framboidal magnetites also suggest that the vein is likely a microfault produced by shock metamorphism. This study attempts to evaluate shock-induced faulting as an analogous process to the faulting that causes earthquakes on Earth. The stresses applied to such faults can be expressed by the following equation based on a fault mechanics analysis³⁹:

$$\tau = \frac{\Delta T C d \rho}{D} \quad (1)$$

where τ , ΔT , C , d , ρ and D are the frictional shear stress, temperature increase, heat capacity of bulk rock, fault thickness, density of bulk rock and displacement along the fault, respectively. The frictional shear stress is converted into the mean stress P_m ($[\sigma_1 + \sigma_3]/2$; $\sigma_1 > \sigma_2 \approx \sigma_3$) using the following equation⁴⁰:

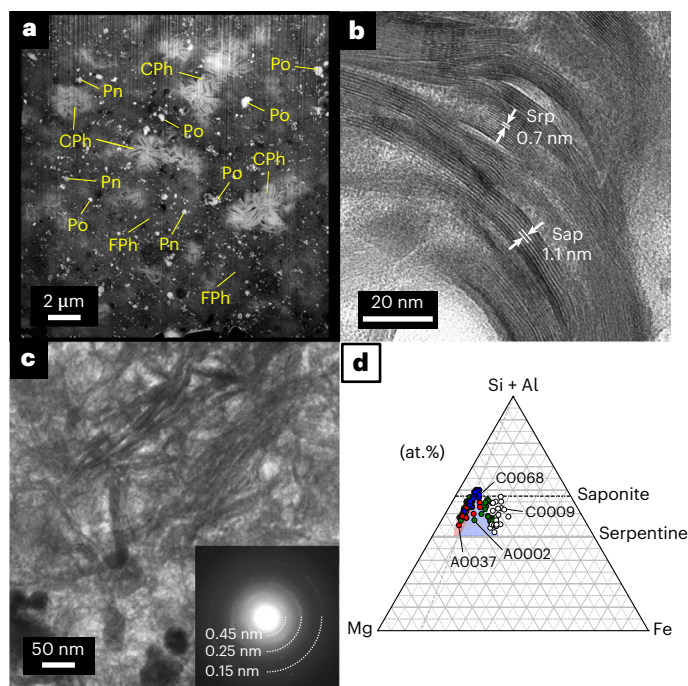


Fig. 3 | Typical mineralogy of Ryugu particles under a transmission electron microscope. **a**, High-angle annular dark-field scanning TEM image of an ultrathin section of C0068. CPh, coarse-grained phyllosilicate aggregate; FPh, fine-grained phyllosilicates matrix; Pn, pentlandite; Po, pyrrhotite. **b**, Bright-field TEM image of serpentine (Srp)–saponite (Sap) intergrowth in A0037. Srp and Sap show interlayer spacings of 0.7 and 1.1 nm, respectively. **c**, Bright-field TEM image of poorly crystalline phyllosilicates in C0068. The SAED pattern shows powder diffraction rings corresponding to the d spacings of 0.45, 0.25 and 0.15 nm from the portion that is shown in the inset. **d**, The Mg–(Si + Al)–Fe ternary plot of phyllosilicates in particles A0002, A0037, C0009 and C0068. The black broken lines show the solid–solution lines for Srp and Sap. Chemical compositional ranges of coarse- and fine-grained phyllosilicates in the Orgueil CI chondrite³⁴ are shown as the light red area and light blue area, respectively. The grey broken line shows the Mg/(Mg + Fe) trend of phyllosilicates of A0037 and C0068 with 0.84. Highly Fe-rich compositions in particles A0002 and C0009 are probably caused by submicrometer-scale Fe sulfide grains within the phyllosilicate grains, which cannot be excluded by the spatial resolution of the scanning TEM–energy dispersive X-ray spectroscopy (EDS) analysis and/or Mg–Fe heterogeneity in the phyllosilicates themselves. The data with higher Si contents than Sap would be caused by the presence of nanometre-scale Si-rich amorphous materials in the interstices of the phyllosilicate layers. Numbers of analyses: $N = 44$ for A0002, $N = 19$ for A0037, $N = 20$ for C0009 and $N = 27$ for C0068.

$$\tau = \frac{\mu}{\sqrt{1 + \mu^2}} P_m \quad (2)$$

where μ denotes the friction coefficient. Here, ΔT corresponds to localized temperature increase only at the microfault zone. We assume that the maximum ΔT of $\sim 1,100$ K is between the lowest Ryugu surface temperature (~ 300 K)⁴¹ and the solidus temperature of hydrated carbonaceous chondrites corresponding to the upper temperature limit of frictional heating without melting ($\sim 1,400$ K)⁴². The friction coefficient μ was set to 0.1 as a typical value in the high-speed friction of serpentine–clay-rich rocks^{43,44}. C ($865 \text{ J kg}^{-1} \text{ K}^{-1}$)³¹ and ρ (1.79 g cm^{-3})³¹ values are assumed to be those of typical Ryugu particles. D ($48.9 \mu\text{m}$) and d ($5.3 \mu\text{m}$) are estimated values from the observed dimensions of a deformed spherical framboidal magnetite aggregate (details are in Methods). By inserting the above parameters into equations (1) and (2), the upper bound of the mean stress, which is approximated as the peak pressure, is roughly 2 GPa (Fig. 5 and Methods). The particle C0014 could be an ejecta from the artificial impact crater made by the SCI. It

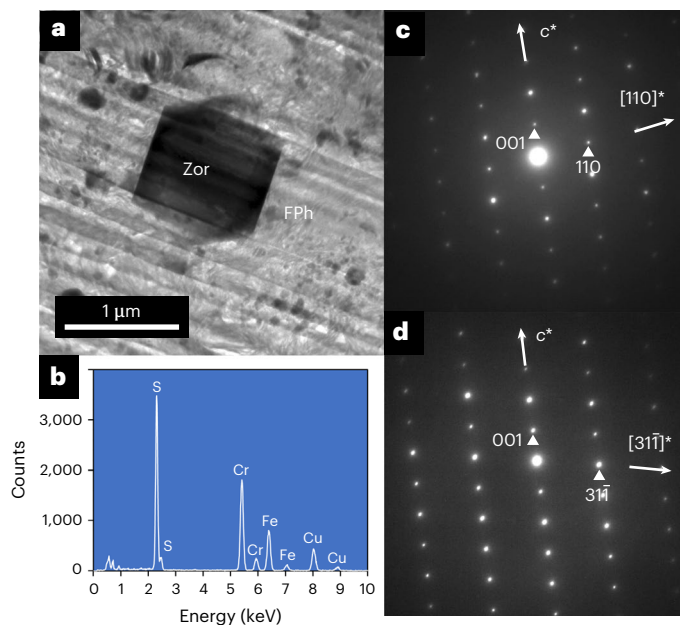


Fig. 4 | High-pressure phase of FeCr_2S_4 . **a**, Bright-field TEM image of an Fe sulfide grain (Zor) embedded in FPh particle A0002. **b**, X-ray spectrum from the grain in **a** showing pure FeCr_2S_4 composition. The Cu peaks in the EDS spectrum in **b** are from the copper grid used for handling/placement of the FIB section. **c,d**, SAED patterns from the FeCr_2S_4 grain with the monoclinic NiAs structure (zolenskyite) along the $[110]$ (**c**) and $[1\bar{3}0]$ (**d**) zone axes. Arrows denote the directions of reciprocal lattice vectors $[uvw]^*$. c^* denotes a reciprocal lattice axis.

could be suggested that the microfault-like veins were produced by shock deformation during the SCI cratering operation. However, the possibility of microfaulting being caused by the impact of the SCI can be ruled out because only <0.003 vol% of SCI ejecta would experience >2 GPa of pressure based on shock physics calculations (Supplementary Figs. 8–10).

Submicrometer-scale observations also provide evidence concerning the peak temperature and pressure experienced by Ryugu particles. Even at the TEM scale, we could not find any dehydration and melting textures of Mg–Fe phyllosilicates, such as abundant vesicles and the formation of fine Fe sulfide/oxide particles embedded in Si-rich amorphous silicate, which were reported in an experimentally shocked hydrated chondrite³⁷. This suggests that the heating temperature did not exceed ~ 500 °C, which corresponds to the dehydration temperature of Mg–Fe–serpentine⁴⁵ (Supplementary Fig. 4). As recently reported, the stabilities of aliphatic carbon-rich organics and cubanite (CuFe_2S_3) found in Ryugu materials also provide constraints on the upper temperature bound to 30 °C (ref. 27) and 210 °C (ref. 32), respectively. The detailed shock-induced thermal history of Ryugu’s materials is uncertain since the cooling process after shock heating depends on the impactor/target body sizes. Aliphatic carbon and cubanite, which are stable at low-temperature conditions, could be retained if the duration of high-temperature shock heating was very short (for example, seconds to hours) and fluctuated extensively. In contrast, phyllosilicates as the most abundant component are susceptible even within microseconds of shock heating and are dehydrated at >580 °C (ref. 24). Therefore, the peak temperature constraint from Mg–Fe–serpentine is more reliable. Previous hydrocode impact simulations of serpentine-rich materials were optimized to investigate the peak pressure and peak temperature relations of both CM carbonaceous chondrites (dominated by Mg–Fe phyllosilicates) and CI chondrites⁴⁶. When the shock impedance of the CI-like Ryugu materials is adapted from that of CM chondrites, the

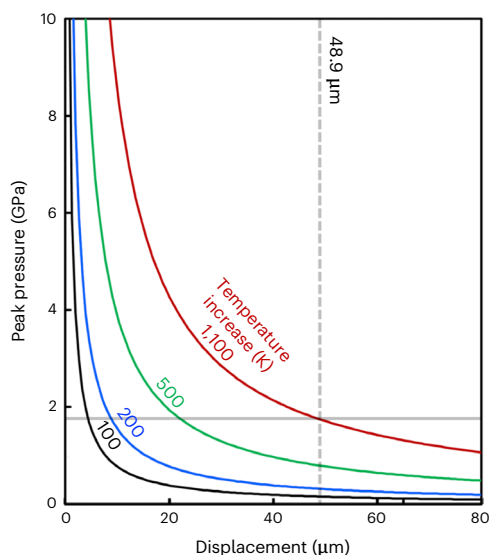


Fig. 5 | The displacement–pressure–temperature relations of the microfault.

The numbers beside each curve represent temperature increase (Kelvin) at the microfault zone. The observed displacement along the fault is estimated to be 48.9 μm . Although average peak temperature is estimated to be below $-500\text{ }^\circ\text{C}$ based on non-dehydration of Mg–Fe–serpentine⁴⁵, a much higher temperature is expected within shear zones due to frictional heating. Given that the upper bound of the peak temperature is $-1,100\text{ }^\circ\text{C}$ considering the solidus temperature of bulk carbonaceous chondrite⁴², the peak pressure in the Ryugu particle is estimated to be below -2 GPa .

upper bound of the peak pressure for the Ryugu materials is -5 GPa (Supplementary Fig. 4).

The discovery of a unique Fe sulfide phase (zolenskyite) in particle A0002 strongly constrains the peak pressure. The phase equilibrium of FeCr_2S_4 has been investigated experimentally⁴⁷ (Supplementary Fig. 5). Daubr elilite is stable at ambient pressure and room temperature. At $700\text{ }^\circ\text{C}$, a disordered hexagonal NiAs-type phase was stable above -4 GPa , and the transition pressure increased with decreasing temperature. The study also reported that an ordered monoclinic NiAs-type phase (zolenskyite) was recovered at $520\text{ }^\circ\text{C}$ and 5.5 GPa . Although the precise phase relations of the hexagonal and monoclinic phases have not been clarified in detail, the higher density of zolenskyite (4.09 g cm^{-3})³⁸ compared with daubr elilite (3.83 g cm^{-3})⁴⁸ suggests that zolenskyite is a high-pressure phase of FeCr_2S_4 . Considering the maximum shock-heating temperature of $-500\text{ }^\circ\text{C}$ for Ryugu particles as a whole, which was deduced from the survival of phyllosilicates, daubr elilite would have transformed into zolenskyite in A0002 close to 2 GPa .

Recent high-resolution TEM analysis reported that some surfaces of Ryugu particles have space weathering features caused by solar wind irradiation and/or (micro-)meteorite bombardment⁴⁹. Amongst them, the outermost frothy layer is interpreted as the melting products of the phyllosilicates-rich matrix by the latter process on Ryugu’s surface. The shock effects are limited to near-surface portions of $<1\text{ }\mu\text{m}$ in thickness; therefore, they do not represent the shock features of the whole particle. In the present study, we conclude that the average peak pressure of the Ryugu particles is -2 GPa , corresponding to an impact velocity of -1 km s^{-1} , based on petrological and mineralogical shock-related features (Supplementary Figs. 4 and 6); it should be also noted that the estimated peak pressure could have some uncertainty.

The occurrence of hydrothermal minerals, such as phyllosilicates, dolomite, and framboidal magnetite, indicates that the Ryugu surface materials experienced extensive aqueous alteration, as documented for hydrated chondrites^{34,50}. However, the size of Ryugu ($<1\text{ km}$) is too small to maintain internal heat caused by ^{26}Al decay long enough for aqueous alteration to form hydrothermal minerals³¹, indicating that

this asteroid must have originated from a larger precursor parent body. ^{53}Mn – ^{53}Cr dating of carbonates in Ryugu particles suggests that the carbonates formed within 1.8 million years after Ca–Al-rich inclusion formation²⁹, much earlier than estimated in previous studies^{30,33}. This implies that the large precursor body needs to be broken into pieces smaller than 20 km in diameter earlier than or shortly after the carbonate formation age; otherwise, the amount of ^{26}Al in the large body at that time ($^{26}\text{Al}/^{27}\text{Al} = -10^{-5}$) would yield enough heat to cause dehydration of hydrous minerals and then, melting subsequent to aqueous alteration²⁹. Therefore, the present Ryugu, as a rubble-pile hydrated asteroid³², likely formed by the aggregation of fragments from a large impact event on the precursor body before the onset of any extensive thermal metamorphism in this larger body. Alternatively, the Ryugu materials originated following an impact on the CI/CM-like surface layer of a large differentiated precursor body during prograde thermal metamorphism as previously proposed for the asteroid Ceres³³.

Recent impact experiments and hydrocode simulations⁵⁴ modelled the collision of a 20-km -diameter impactor asteroid and a 100-km -diameter target asteroid, both of which are made of hydrated and porous material, thus simulating Ryugu-like materials. Impact-induced volatile release during the collision was limited to only $2\text{--}4\text{ wt}\%$ of the impactor mass, even at a typical impact velocity ($6\text{--}7\text{ km s}^{-1}$) in the main asteroid belt⁵⁵. Summarizing the theoretical and present observational results, most of the masses of collided asteroids would be merely mechanically disrupted without dehydration to form the rubble-pile Ryugu body. Only a small mass near the impact point on a Ryugu precursor body may have been extensively heated above the dehydration temperature of Mg–Fe serpentine and pulverized to comprise partly/completely dehydrated and submillimeter-sized dust particles, along with vapour release, as previously predicted by shock experiments^{23,24}.

The complete lack of dehydration textures and mineral features in Ryugu particles observed in the present study demonstrates that hydrated asteroids preserved their water as hydroxyl in phyllosilicates throughout the impact events that they experienced. This study also suggests that the production of micrometeorites ($<500\text{ }\mu\text{m}$ in size¹⁸) due to shock heating-induced volatilization during such breakup events would be limited to the vicinity of the impact point, and its total amount is much smaller than previously expected²³. Hence, the vast majority of hydrous materials from CI-like asteroids would come to the Earth as meteorites ($>500\text{ }\mu\text{m}$ in size) rather than micrometeorites. This finding appears to be at odds with the fact that most unmelted and partially melted micrometeorites collected on the Earth’s surface have genetic relationships with hydrated CI, CM, and Tagish Lake-like carbonaceous chondrites^{20,21}. A possible explanation to reconcile this discrepancy is the breakup of hydrous meteorites due to aerodynamic heating when entering Earth’s atmosphere^{56,57}. However, solar wind noble gases retained in most of micrometeorites⁵⁸ suggest that those particles kept their original sizes when entering Earth’s atmosphere.

Recent remote-sensing observations of the hydrated asteroid Bennu by National Aeronautics and Space Administration’s OSIRIS REX spacecraft found that particles (centimetre scale or less) were being ejected repeatedly from the surface of the asteroid⁵⁹. We hypothesize that the cracking of surface rocks of the hydrated asteroids due to thermal fracturing is an alternative mechanism to produce a large number of micrometeorites. Further analyses of the returned samples from Bennu will provide more detailed insights into how hydrated asteroids preserve their water and how this water can then be delivered to the Earth.

Methods

SEM

Ryugu’s surface particles collected by the Hayabusa2 spacecraft were recovered from the reentry capsule and transported to the JAXA Curation Facility, Japan, without terrestrial atmospheric exposure²⁵. After

cataloguing and preliminary analysis at the JAXA curation facility, eight particles up to 4.1 mm in size were allocated to the phase 2 curation Kochi team for in-depth investigations. An airtight sample transport vessel with a sample capsule pack made of sapphire glass and stainless steel⁶⁰ was used to avoid terrestrial contaminants during sample transportation among institutes.

The particles were polished under dry conditions to avoid the elution of any material from the surface during polishing. The polished surface of each sample was examined using a scanning electron microscope (JEOL JSM-7100F) equipped with an EDS (Oxford Instruments AZtec Energy) to obtain an overview of the mineralogy and textures of the samples using high-resolution imaging at the National Institute of Polar Research, Japan. The details of the sample transfers, processing and SEM observations are described in Ito et al.²⁷ and Yamaguchi et al.³².

Sample preparation using a focused ion beam instrument

Approximately 150- to 200-nm-thick sections of Ryugu particles were prepared using a focused ion beam (FIB) instrument (Hitachi High-Tech SMI4050) at the Kochi Institute for Core Sample Research (Kochi), Japan Agency for Marine-Earth Science and Technology. All the sections were extracted from unprocessed broken pieces of original particles immediately after removal from airtight sample transport vessels, which were filled with purified N₂ gas. The pieces were mounted on carbon tape and transported to the FIB chamber. After the deposition of tungsten protection layers, regions of interest (up to 25 × 25 μm²) were cut out and thinned using a Ga⁺ ion beam at an accelerating voltage of 30 kV and then, finalized at 5 kV and a probe current of 40 pA to minimize surface ion-damage layers. Subsequently, the ultrathin sections were mounted on scaled-up Cu grids (Kochi grid⁶⁰) using a micromanipulator equipped with an FIB.

TEM

Eleven FIB sections with and without scanning transmission X-ray microscopy-near edge X-ray absorption fine structure spectroscopy (STXM-NEXAFS) and high spatial resolution secondary ion mass spectrometry (NanoSIMS) analyses were examined using a transmission electron microscope (JEOL JEM-ARM200F) operated at an accelerating voltage of 200 kV at Kochi, Japan Agency for Marine-Earth Science and Technology. Microtextural observations were performed by bright-field TEM and high-angle annular dark-field scanning TEM. Mineral phases were identified using SAED and lattice-fringe imaging (high-resolution TEM), and chemical analyses were performed using EDS with a 100-mm² silicon drift detector and the JEOL Analysis Station 4.30 software. For quantitative analyses, the intensities of the characteristic X-rays of each element were measured using a fixed acquisition time of 30 s, beam scan area of 100 × 100 nm², and beam current of 50 pA in the scanning TEM mode. The (Si + Al)-Mg-Fe ratios of the phyllosilicates were determined using experimental thickness-corrected *k* factors obtained from a natural pyrope-almandine garnet standard.

Pressure estimation by microfault analysis

In the present peak pressure estimation by fault mechanics calculations, shear stress on the microfault plane was calculated by equation (1) in the text using the following physical properties for Ryugu particles: 865 J kg⁻¹ K⁻¹ at 298 K for heat capacity *C* and 1.79 g cm⁻³ for density *ρ* (ref. 31). As for temperature increase ΔT , none of decomposition features were recognized in the phyllosilicates in association with the microfault-like vein observed by SEM. This may suggest that the phyllosilicates experienced temperatures below 500 °C⁴⁵. However, in contrast to the entire particle heated to the mean shock temperature, the locally heated portions near the microfault should be cooled more rapidly by thermal conduction to the relatively cold surrounding materials. If the dehydration kinetics of phyllosilicates is sluggish, it is likely that the phyllosilicates were not decomposed even above 500 °C during transient heating by faulting. Therefore, the upper temperature

limit of microfault was set to the solidus temperature of the bulk Ryugu particles (-1,100 °C) in the present calculations.

To estimate the displacement *D* of the microfaulting, we assumed a simple shear model for sphere-ellipsoid deformation. Shear strain γ is expressed by the following equation:

$$\gamma = D/2r_0, \quad (3)$$

where *r*₀ is the radius of the predeformed spherical object. The shear strain γ was calculated using the following equation:

$$(a/b)^2 = \left[(\gamma^2 + 2) + \gamma(\gamma^2 + 4)^{1/2} \right] / \left[(\gamma^2 + 2) - \gamma(\gamma^2 + 4)^{1/2} \right], \quad (4)$$

where *a* and *b* are the long and short axes of an elliptically deformed object, respectively⁶¹. The radius *r*₀ (9.5 μm) of an aggregate of original spherical framboidal magnetite was estimated by measuring the total area of the elongated framboidal magnetite aggregate in an observed backscattered electron image taken from particle C0014 using ImageJ software. The long axis *a* (45.2 μm) and short axis *b* (5.3 μm) of the framboidal magnetite were directly measured by the backscattered electron image. From these measured parameters and equations (3) and (4), the displacement *D* of the microfault was estimated as 48.9 μm. Finally, the mean stress *P*_m was calculated using the frictional shear stress τ from equations (1) and (2), as shown in the text. Although fault mechanics analysis and shock physics calculations are not simply compared with each other, the mean stress *P*_m ($[\sigma_1 + \sigma_3]/2; \sigma_1 > \sigma_2 \approx \sigma_3$) in the former analysis⁴⁰ determined by equations (1) and (2) is comparable with peak pressure termed as the average stress ($[\sigma_1 + 2\sigma_3]/3; \sigma_1 > \sigma_2 \approx \sigma_3$) in the latter analysis⁶².

Recent shock physics calculations using the iSALE code clarified peak pressure and deviatoric stress history in shock metamorphism for the particles in granite as a model target material⁶². The largest component of deviatoric stress is maximized around the timing of peak pressure. In addition, the differential stress becomes a maximum by the time when pressure drops to several tens of percent of the peak pressure. A microfault is likely to be the most displaced immediately after the end of compression phase (that is, at the beginning of decompression phase) because the normal stress to the fault starts to decrease.

Phase identification of zolenskyite

Single-crystal electron diffraction patterns from an FeCr₂S₄ grain were indexed by the zolenskyite unit cell with the space group *C2/m* and lattice parameters *a* = 1.284 nm, *b* = 0.344 nm, *c* = 0.594 nm and $\beta = 117^\circ$ (ref. 38).

Data availability

All data needed to evaluate the conclusions are present in the paper and Supplementary Information. They will also be put on the Japan Aerospace Exploration Agency Data Archives and Transmission System (<https://www.darts.isas.jaxa.jp/curation/hayabusa2>) after a 1-year proprietary period. Source data are provided with this paper.

References

- Gillet, P. & El Goresy, A. Shock events in the Solar System: the message from minerals in terrestrial planets and asteroids. *Annu. Rev. Earth Planet. Sci.* **41**, 257–285 (2013).
- Stöfler, D., Hamann, C. & Metzler, K. Shock metamorphism of planetary silicate rocks and sediments: proposal for an updated classification system. *Meteorit. Planet. Sci.* **53**, 5–49 (2018).
- McSween, H. Y. *Meteorites and Their Parent Planets* (Cambridge University Press, 1999).
- Sharp, T. G. & Decarli, P. in *Meteorites and the Early Solar System II* (eds Lauretta, D. S. & McSween, H. Y.) 653–677 (Univ. of Arizona Press, 2006).

5. Bischoff, A., Schleiting, M., Wieler, R. & Patzek, M. Brecciation among 2280 ordinary chondrites: constraints on the evolution of their parent bodies. *Geochim. Cosmochim. Acta* **238**, 516–541 (2018).
6. Miyahara, M. et al. Systematic investigations of high-pressure polymorphs in shocked ordinary chondrites. *Meteorit. Planet. Sci.* **55**, 2619–2651 (2020).
7. Ohtani, E. et al. Formation of high-pressure minerals in shocked L6 chondrite Yamato 791384: constraints on shock conditions and parent body size. *Earth Planet. Sci. Lett.* **227**, 505–515 (2004).
8. Xie, Z., Sharp, T. G. & DeCarli, P. S. High-pressure phases in a shock-induced melt vein of the Tenham L6 chondrite: constraints on shock pressure and duration. *Geochim. Cosmochim. Acta* **70**, 504–515 (2006).
9. Kaneko, S. et al. Discovery of stishovite in Apollo 15299 sample. *Am. Mineral.* **100**, 1308–1311 (2015).
10. Crow, C. A., Moser, D. E. & McKeegan, K. D. Shock metamorphic history of >4 Ga Apollo 14 and 15 zircons. *Meteorit. Planet. Sci.* **54**, 181–201 (2018).
11. Zolensky, M. et al. Mineralogy and petrology of comet 81P/Wild2 nucleus samples. *Science* **314**, 1735–1739 (2006).
12. Tomeoka, K., Tomioka, N. & Ohnishi, I. Silicate minerals and Si-O glass in Comet Wild 2 samples: transmission electron microscope study. *Meteorit. Planet. Sci.* **43**, 273–284 (2008).
13. Nakamura, T. et al. Itokawa dust particles: a direct link between S-type asteroids and ordinary chondrites. *Science* **333**, 1113–1116 (2011).
14. Nakamura, E. et al. Space environment of an asteroid preserved on micrograins returned by the Hayabusa spacecraft. *Proc. Natl Acad. Sci. USA* **109**, E624–E629 (2012).
15. Noguchi, T. et al. An attempt to identify minerals in the Itokawa dust particles by micro-Raman spectroscopy. *Bunseki Kagaku* **61**, 299–310 (2012).
16. Zolensky, M. et al. Measuring the shock stage of Itokawa and asteroid regolith grains by electron backscattered diffraction, optical petrography, and synchrotron X-ray diffraction. *Meteorit. Planet. Sci.* **57**, 1060–1078 (2022).
17. Genge, M. J., Grady, M. & Hutchison, R. The textures and compositions of fine-grained Antarctic micrometeorites: implications for comparisons with meteorites. *Geochim. Cosmochim. Acta* **61**, 5149–5162 (1997).
18. Engrand, C. & Maurette, M. Carbonaceous micrometeorites from Antarctica. *Meteorit. Planet. Sci.* **33**, 565–580 (1998).
19. Taylor, S., Lever, J. H. & Harvey, R. P. Accretion rate of cosmic spherules measured at the South Pole. *Nature* **392**, 899–903 (1998).
20. Nakamura, T., Noguchi, T., Yada, T., Nakamura, Y. & Takaoka, N. Bulk mineralogy of individual micrometeorites determined by X-ray diffraction analysis and transmission electron microscopy. *Geochim. Cosmochim. Acta* **65**, 4385–4397 (2001).
21. Noguchi, T., Nakamura, T. & Nozaki, W. Mineralogy of phyllosilicate-rich micrometeorites and comparison with Tagish Lake and Sayama meteorites. *Earth Planet. Sci. Lett.* **202**, 229–246 (2002).
22. Scott, E. R. D., Keil, K. & Stöffler, D. Shock metamorphism of carbonaceous chondrites. *Geochim. Cosmochim. Acta* **56**, 4281–4293 (1992).
23. Tomeoka, K., Kiriya, K., Nakamura, K., Yamahana, Y. & Sekine, T. Interplanetary dust from the explosive dispersal of hydrated asteroids by impacts. *Nature* **423**, 60–62 (2003).
24. Tomioka, N., Tomeoka, K., Nakamura-Messenger, K. & Sekine, T. Heating effects of the matrix of experimentally shocked Murchison CM chondrite: comparison with micrometeorites. *Meteorit. Planet. Sci.* **42**, 19–30 (2007).
25. Yada, T. et al. Preliminary analysis of the Hayabusa2 samples returned from C-type asteroid Ryugu. *Nat. Astron.* **6**, 214–220 (2022).
26. Greenwood, R. C. et al. Oxygen isotope evidence from Ryugu samples for early water delivery to Earth by CI chondrites. *Nat. Astron.* **7**, 29–38 (2023).
27. Ito, M. et al. A pristine record of outer Solar System materials from asteroid Ryugu's returned sample. *Nat. Astron.* **6**, 1163–1171 (2022).
28. Liu, M.-C. et al. Incorporation of ¹⁶O-rich anhydrous silicates in the protolith of highly hydrated asteroid Ryugu. *Nat. Astron.* **6**, 1172–1177 (2022).
29. McCain, K. A. et al. Early fluid activity on Ryugu inferred by isotopic analyses of carbonates and magnetite. *Nat. Astron.* **7**, 309–317 (2023).
30. Nakamura, E. et al. On the origin and evolution of the asteroid Ryugu: a comprehensive geochemical perspective. *Proc. Jpn. Acad. Ser. B* **98**, 227–282 (2022).
31. Nakamura, T. et al. Formation and evolution of carbonaceous asteroid Ryugu: direct evidence from returned samples. *Science* **379**, eabn8671 (2022).
32. Yamaguchi, A. et al. Insight into multistep geological evolution of C-type asteroids from Ryugu particles. *Nat. Astron.* <https://doi.org/10.1038/s41550-023-01925-x> (2023).
33. Yokoyama, T. et al. Samples returned from the asteroid Ryugu are similar to Ivuna-type carbonaceous meteorites. *Science* **379** <https://doi.org/10.1126/science.abn7850> (2022).
34. Tomeoka, K. & Buseck, P. R. Matrix mineralogy of the Orgueil CI carbonaceous chondrite. *Geochim. Cosmochim. Acta* **52**, 1627–1640 (1988).
35. King, A. J., Schofield, P. F., Howard, K. T. & Russell, S. S. Modal mineralogy of CI and CI-like chondrites by X-ray diffraction. *Geochim. Cosmochim. Acta* **165**, 148–160 (2015).
36. Alving, J., Patzek, M. & Bischoff, A. Modal abundances of coarse-grained (>5 μm) components within CI-chondrites and their individual clasts: mixing of various lithologies on the CI parent body(ies). *Geochemistry* **79**, 125532 (2019).
37. Tomeoka, K., Yamahana, Y. & Sekine, T. Experimental shock metamorphism of the Murchison CM carbonaceous chondrite. *Geochim. Cosmochim. Acta* **63**, 3683–3703 (1999).
38. Ma, C. & Rubin, A. E. Zolenskyite, FeCr₂S₄, a new sulfide mineral from the Indarch meteorite. *Am. Mineral.* **107**, 1030–1033 (2022).
39. Kanamori, H., Anderson, D. L. & Heaton, T. H. Frictional melting during the rupture of the 1994 Bolivian earthquake. *Science* **279**, 839–842 (1998).
40. Jaeger, J. C., Cook, N. G. & Zimmerman, R. *Fundamentals of Rock Mechanics* (Wiley, 2009).
41. Sugita, S. et al. The geomorphology, color, and thermal properties of Ryugu: implications for parent-body processes. *Science* **364**, eaaw0422 (2019).
42. Jurewicz, A. J. G., Mittlefehldt, D. W. & Jones, J. H. Experimental partial melting of the Allende (CV) and Murchison (CM) chondrites and the origin of asteroidal basalts. *Geochim. Cosmochim. Acta* **57**, 2123–2139 (1993).
43. Hirose, T. & Bystricky, M. Extreme dynamic weakening of faults during dehydration by coseismic shear heating. *Geophys. Res. Lett.* **34**, L14311 (2007).
44. Di Toro, G. et al. Fault lubrication during earthquakes. *Nature* **471**, 494–498 (2011).
45. Akai, J. T-T diagram of serpentine and saponite, and estimation of metamorphic heating degree of antarctic carbonaceous chondrites. *Proc. NIPR Symp. Antarct. Meteor.* **5**, 120–135 (1992).
46. Bland, P. A. et al. Pressure-temperature evolution of primordial solar system solids during impact-induced compaction. *Nat. Commun.* **5**, 5451 (2014).

47. Tressler, R. E., Hummel, F. A. & Stubican, V. S. Pressure-temperature study of sulfospinel. *J. Am. Ceram. Soc.* **51**, 648–651 (1968).
48. Raccach, P. M., Bouchard, R. J. & Wold, A. Crystallographic study of chromium spinels. *J. Appl. Phys.* **37**, 1436–1437 (1966).
49. Noguchi, T. et al. A dehydrated space weathered skin cloaking the hydrated interior of Ryugu. *Nat. Astron.* **7**, 170–181 (2023).
50. Brearley, A. in *Meteorites and the Early Solar System II* (eds Lauretta, D. S. & McSween, H. Y.) 587–624 (Univ. of Arizona Press, 2006).
51. Grimm, R. E. & McSween, H. Y. Heliocentric zoning of the asteroid belt by aluminum-26 heating. *Science* **259**, 653–655 (1993).
52. Morota, T. et al. Sample collection from asteroid (162173) Ryugu by Hayabusa2: implications for surface evolution. *Science* **368**, 654–659 (2020).
53. McSween, H. Y. et al. Carbonaceous chondrites as analogs for the composition and alteration of Ceres. *Meteorit. Planet. Sci.* **53**, 1793–1804 (2018).
54. Kurosawa, K. et al. Ryugu's observed volatile loss did not arise from impact heating alone. *Commun. Earth Environ.* **2**, 146 (2021).
55. Bottke, W. F., Nolan, M. C., Greenberg, R. & Kolvoord, R. A. Velocity distributions among colliding asteroids. *Icarus* **107**, 255–268 (1994).
56. Baldwin, B. & Sheaffer, Y. Ablation and breakup of large meteoroids during atmospheric entry. *J. Geophys. Res.* **76**, 4653–4668 (1971).
57. Popova, O. et al. Very low strengths of interplanetary meteoroids and small asteroids. *Meteorit. Planet. Sci.* **46**, 1525–1550 (2011).
58. Okazaki, R. et al. Mineralogy and noble gas isotopes of micrometeorites collected from Antarctic snow. *Earth Planets Space* **67**, 90 (2015).
59. Hergenrother, C. W., Adam, C. D., Chesley, S. R. & Lauretta, D. S. Introduction to the special issue: exploration of the activity of asteroid (101955) Bennu. *J. Geophys. Res. Planets* **125**, e2020JE006549 (2020).
60. Ito, M. et al. The universal sample holders of microanalytical instruments of FIB, TEM, NanoSIMS, and STXM-NEXAFS for the coordinated analysis of extraterrestrial materials. *Earth Planets Space* **72**, 133 (2020).
61. Ramsay, J. G. Shear zone geometry: a review. *J. Struct. Geol.* **2**, 83–99 (1980).
62. Rae, A. S. P., Poelchau, M. H. & Kenkmann, T. Stress and strain during shock metamorphism. *Icarus* **370**, 114687 (2021).

Acknowledgements

We thank all the scientists and engineers of the Hayabusa2 project for their dedication and skills to bring these precious particles back to Earth from the asteroid Ryugu. We also thank Marine Works Japan for the assistance of curative activity, initial non-destructive investigation and sample preparation of Ryugu particles. We thank the developers of iSALE, including G. Collins, K. Wünnemann, B. Ivanov, J. Melosh and D. Elbeshausen. We also thank T. Davison for the development of pySALEPlot. The shock physics modelling was in part carried out on PC cluster at the Center for Computational Astrophysics, National Astronomical Observatory of Japan. This research was supported in part by the JSPS KAKENHI (Grants JP20H01965 to N.T.; JP18K18795 and JP18H04468 to M.I.; JP19H01959 to A.Y.; JP18H05479 (Innovative Areas MFS Materials Science) to M.U.; JP18K03729 to M.K.; JP21K03652 to N.I.; JP17H06459 to T.U.; JP19K03958 to M.A.; JP17H06459 to T. Ohigashi; JP18K03830 to T.Y.; JP17H06459 and JP19H01951 to S.-i.W.;

and JP18KK0092, JP19H00726, JP21K18660 and JP21H01140 to K.K.) and by the National Institute of Polar Research Research Project (Grant KP307 to A.Y.).

Author contributions

N.T., M.I. and A.Y. organized the research project. N.T., M.I., A.Y., M.U., N.I., N.S., T. Ohigashi, M.K. M-C.L., R.C.G., K.U., A.N., K.Y., H.Y. and Y. Kodama conducted sample handling, preparation and mounting processes of Ryugu grains. M.I., N.T., T. Ohigashi, M.U., K.U., H.Y., Y. Kodama, K.H., I.S., I.O. and Y. Karouji developed universal sample holders for multiple instruments. Scanning electron microscopy analysis was conducted by A.Y., M.K., N.I., M.I. and N.T. Focused ion beam sample processing was conducted by Y. Kodama and N.T. Transmission electron microscopy work was done by N.T. Fault mechanics calculations were conducted by N.T. and K.O., and peak pressure caused by the small carry-on impactor was evaluated by K.K. T.N., A. Miyake, M.M., Y.S. T.M. and Y.I. provided valuable comments and discussion on the mineralogy of Ryugu particles and carbonaceous chondrites. A.N., K.Y., A. Miyazaki, M.N., T.Y., T. Okada, M.A. and T.U. led the JAXA curation activities for initial characterization of allocated Ryugu particles. S.N., T.S., S.T., F.T., M.Y., S.-i.W. and Y.T. administered the project and acted as principal investigators. N.T. wrote the paper, and all the authors discussed the results and commented on the paper.

Competing interests

The authors declare no competing interests.

Additional information

Supplementary information The online version contains supplementary material available at <https://doi.org/10.1038/s41550-023-01947-5>.

Correspondence and requests for materials should be addressed to Naotaka Tomioka.

Peer review information *Nature Astronomy* thanks Christopher Hamann and the other, anonymous, reviewer(s) for their contribution to the peer review of this work.

Reprints and permissions information is available at www.nature.com/reprints.

Publisher's note Springer Nature remains neutral with regard to jurisdictional claims in published maps and institutional affiliations.

Open Access This article is licensed under a Creative Commons Attribution 4.0 International License, which permits use, sharing, adaptation, distribution and reproduction in any medium or format, as long as you give appropriate credit to the original author(s) and the source, provide a link to the Creative Commons license, and indicate if changes were made. The images or other third party material in this article are included in the article's Creative Commons license, unless indicated otherwise in a credit line to the material. If material is not included in the article's Creative Commons license and your intended use is not permitted by statutory regulation or exceeds the permitted use, you will need to obtain permission directly from the copyright holder. To view a copy of this license, visit <http://creativecommons.org/licenses/by/4.0/>.

© The Author(s) 2023

¹Kochi Institute for Core Sample Research, X-star, Japan Agency for Marine-Earth Science and Technology, Nankoku, Japan. ²National Institute of Polar Research, Tachikawa, Japan. ³The Graduate University for Advanced Studies, Hayama, Japan. ⁴Japan Synchrotron Radiation Research Institute, Sayo, Japan. ⁵Graduate School of Science, Department of Chemistry, Tokyo Metropolitan University, Hachioji, Japan. ⁶Department of Chemistry,

Faculty of Science, Kanagawa University, Hiratsuka, Japan. ⁷UVSOR Synchrotron Facility, Institute for Molecular Science, Okazaki, Japan. ⁸Institute of Materials Structure Science, High Energy Accelerator Research Organization, Tsukuba, Japan. ⁹Department of Earth, Planetary, and Space Sciences, University of California, Los Angeles, CA, USA. ¹⁰Planetary and Space Sciences, The Open University, Milton Keynes, UK. ¹¹Institute of Space and Astronautical Science, Japan Aerospace Exploration Agency, Sagami-hara, Japan. ¹²Marine Works Japan, Ltd., Yokosuka, Japan. ¹³Department of Mechanical Engineering, Osaka University, Suita, Japan. ¹⁴Synchrotron Radiation Research Center, Nagoya University, Nagoya, Japan. ¹⁵Earth and Planetary Systems Science Program, Graduate School of Advanced Science and Engineering, Hiroshima University, Higashi-Hiroshima, Japan. ¹⁶Planetary Exploration Research Center, Chiba Institute of Technology, Narashino, Japan. ¹⁷Division of Earth and Planetary Sciences, Kyoto University, Kyoto, Japan. ¹⁸Department of Geosciences, Osaka Metropolitan University, Osaka, Japan. ¹⁹Kanagawa Institute of Technology, Atsugi, Japan. ²⁰Graduate School of Environmental Studies, Nagoya University, Nagoya, Japan. ²¹Present address: Lawrence Livermore National Laboratory, Livermore, CA, USA. ²²Present address: Toyo Corporation, Tokyo, Japan. ✉e-mail: tomioka@jamstec.go.jp